Simulation of toroidal drift mode turbulence driven by temperature gradients and electron trapping

SIMULATION OF TOROIDAL DRIFT MODE TURBULENCE DRIVEN BY TEMPERATURE GRADIENTS AND ELECTRON TRAPPING

H. NORDMAN, J. WEILAND, A. JARMÉN
Institute for Electromagnetic Field Theory,
Chalmers University of Technology
and
Euratom-NFR Association,
Göteborg, Sweden

ABSTRACT. Turbulence and transport due to fully toroidal ion temperature gradient driven drift waves and a collisionless trapped electron mode have been studied by mode coupling simulations and with the quasi-linear theory. Diffusion coefficients in good agreement with the simulations have been obtained. The observed tendency for equilibration of the temperature and density scale lengths leads to particle or heat pinch effects that are in agreement with experimental trends.

1. INTRODUCTION

Transport in the high density regime of tokamaks has recently attracted strong interest [1–3]. A number of experimental results, such as the saturation of the neo-Alcator scaling with density at energy confinement times much shorter than neoclassical [4] and improved energy confinement for peaked density profiles, are apparently explained by theory [5, 6]. Also the improvement of energy confinement for very flat density profiles (H-mode) seems to be reasonable from a theoretical point of view, although this is particularly sensitive to the ion temperature profile [3, 7–11]. The mode involved in explaining high density transport is of a very fundamental nature in that it limits the ratio η of density to temperature scale lengths. The instability is of a reactive fluid type which involves the whole plasma and is independent of dissipation. Although often classified as a drift mode, this instability has its maximum growth rate for wavelengths much larger than the ion Larmor radius; this enhances the transport. Since the minimum threshold for η_i is typically around 1 for $T_e = T_i$ when kinetic [9] or fully toroidal [12] fluid models are used, the instability has a tendency to equilibrate L_{Ti} and L_n ($L_j = (d \ln j/dr)^{-1}$), thereby adjusting the profiles towards marginal stability [13]. This can also be considered as a mechanism for profile consistency [14]. As long as a purely dissipation free model is used without electron trapping, this equilibration is accomplished only with outgoing heat flux. In the presence of dissipation, however, the slab branch of the η_i mode can lead to inward particle diffusion in the edge region, thereby speeding up the equilibration [15, 16].

The anomalous equilibration of the inhomogeneity scales L_n and L_T on a time-scale shorter than that of the overall relaxation is similar to the equilibration of T_e and T_i in large systems and makes sense as regards thermodynamics. It is, however, not possible to obtain particle transport with the ideal η_i mode theory, which can also not reproduce equilibration or even overall relaxation when $L_T > L_n$ ($\eta < 1$). However, when electron trapping is included, the situation is different.

Previous work on trapped electron modes has considered modes driven by the combined effects of electron trapping and non-adiabatic ion response [17–19], or the effects of temperature gradients have been expressed by general kinetic formulations [20].

It seems that Liu [20] was actually the first author who pointed out the destabilizing effects of temperature gradients on toroidal modes. The article by Liu contains both the toroidal η_i mode and the trapped electron mode in an implicit formulation and provides the foundation for the system studied by us.

In the present work we have included the impact of electron trapping in the collisionless limit on the toroidal ion temperature gradient mode. For this we have used a fully toroidal fluid model [12, 21] that was previously used for the pure η_i mode [3, 11, 12], treating ions and trapped electrons in a symmetrical way. We thereby obtain a system of fourth degree, containing two reactive fluid instabilities — the η_i mode enhanced by electron trapping (ubiquitous mode) and a collision-

less trapped electron mode. The latter mode has a dispersion relation similar to that of the toroidal η_e mode [7], but it occurs for wavelengths much longer than the ion Larmor radius.

The new system also contains the equilibration for $L_T > L_n$ ($\eta < 1$) and the overall relaxation for a small enough ratio L_n/L_B. Furthermore, the system gives rise to particle or heat pinch effects when these are needed to speed up the relaxation. Such effects have been observed experimentally for a long time and are discussed in Refs [15, 16, 22, 23].

The heat pinch effects for $\eta_e \sim \eta_i = \eta$ occur for $\eta \ll 1$. In this regime, each of the uncoupled branches is stable. The instability in this regime is due to coupling between the branches and is driven by compressibility effects that would be stabilizing for uncoupled branches.

The fluid model used is in good agreement with kinetic theory [24] and is valid for arbitrary L_n/L_B. This model has made it possible to perform fully nonlinear mode coupling simulations; such simulations have been done previously for the pure η_i mode [11], and we use them for the full system containing the η_i branch and the trapped electron branch. Good agreement between mode coupling simulations and quasilinear theory has been obtained.

2. FORMULATION

We apply here the two-fluid theory, previously developed to study the pure η_i mode [11], to the trapped electrons as well as to the ions. For the ion fluid, the continuity and energy equations are written

$$\frac{\partial n_i}{\partial t} + \nabla \cdot (n_i \vec{v}_E) + \nabla \cdot (n_i \vec{v}_{*i}) + \nabla \cdot [n_i (\vec{v}_{\pi i} + \vec{v}_{pi})] = 0 \quad (1)$$

$$\frac{3}{2} n_i \left(\frac{\partial}{\partial t} + \vec{v}_i \cdot \nabla \right) T_i + p_i \nabla \cdot \vec{v}_i = - \nabla \cdot \vec{q}_i \quad (2)$$

where

$$\vec{v}_E = \frac{c}{B} (\vec{e} \times \nabla \phi), e = \frac{\vec{B}}{B},$$

$$\vec{v}_{*i} = \frac{c}{e n B} (\vec{e} \times \nabla P)$$

is the ion diamagnetic drift, $\vec{v}_{\pi i}$ is the stress tensor drift, $\vec{v}_{pi}$ is the ion polarization drift, and $\vec{q}_i$ is the diamagnetic ion heat flow $\vec{q}_i^*$:

$$\vec{q}_i^{\,*} = \frac{5}{2} \frac{p_j}{m_i \omega_{ci}} (\vec{e} \times \nabla \delta T_i) \quad (3)$$

This fulfils the condition

$$\nabla \cdot \vec{q}_i^{\,*} = - \frac{5}{2} n \vec{v}_{*i} \cdot \nabla T_i + \frac{5}{2} n \vec{v}_{Di} \cdot \nabla T_i \quad (4)$$

where $\vec{v}_D$ is the magnetic drift (sum of ∇B and curvature drift). Thus, $\nabla \cdot \vec{q}_i$ contributes to the other curvature terms in Eq. (2). Parallel ion motion is neglected in this model. This is reasonable for the fastest growing modes at $k^2\rho^2 \sim 0.1$. For smaller values of $k^2\rho^2$ the growth rate decreases and turns into a damping rate when kinetic effects are included (ion Landau damping). This effect is modelled in the simulations as a low k damping. For large values of $k^2\rho^2$ the damping associated with perpendicular ion viscosity is included.

The trapped electrons are treated as a fluid with an associated perturbation of density (δn_{et}) and temperature (δT_{et}). Since it is found that the trapped electrons do not contribute to the parallel current ($\nabla \cdot (n \vec{v}_{te}) = 0$), the description of the electrons is similar to that for ions (Eqs (1, 2)):

$$\frac{\partial n_{et}}{\partial t} + \nabla \cdot (n_{et} \vec{v}_E) + \nabla \cdot (n_{et} \vec{v}_{*e}) = 0 \quad (5)$$

$$\frac{3}{2} n_e \left(\frac{\partial}{\partial t} + \vec{v}_e \cdot \nabla \right) T_e + p_e \nabla \cdot \vec{v}_e = - \nabla \cdot \vec{q}_e \quad (6)$$

For the electrons, the finite Larmor radius (FLR) effects have been omitted.

Here, the electron magnetic drift v_{De} should be interpreted as a bounce averaged drift. The total electron response can be written

$$\frac{\delta n_e}{n_0} = f_t \frac{\delta n_{et}}{n_{et}} + (1 - f_t) \frac{\delta n_{ef}}{n_{ef}} \quad (7)$$

where n_{ef} is the density of free (passing) electrons and f_t is the fraction of trapped electrons n_{et}. The passing electrons are allowed to reach a Boltzmann distribution

$$\frac{\delta n_{ef}}{n_{ef}} = \frac{e\phi}{T_e} \quad (8)$$

Using quasi-neutrality,

$$\delta n_i = \delta n_{ef} + \delta n_{et} \tag{9}$$

the ion density perturbation can be eliminated from Eqs (1, 2) and we are left with four evolution equations for the perturbation fields. A numerical simulation of the time evolution of the system is described in Section 5. The non-linearities retained are the convective $\vec{E} \times \vec{B}$ non-linearity and the Hasegawa-Mima non-linearity associated with the ion polarization drift.

3. LINEAR DISPERSION RELATION

In Ref. [12] it is shown how a local linear dispersion relation results for the pure η_i mode in the electrostatic limit when parallel ion motion is neglected. In the electrostatic case the same dispersion relation is obtained by neglecting parallel ion motion in the strong ballooning limit [7].

The same result is obtained when electron trapping effects are included [25]. This leads to the modes with the largest growth rates, and the curvature terms have to be evaluated at the symmetry point at the outside of the flux surface. It is straightforward to take the strong ballooning limit for the present system. The dispersion relation thus obtained can be written in the form

$$\frac{\omega_{*e}}{N_i}\left[\omega(1-\varepsilon_n) - \left(\frac{7}{3} - \eta_i - \frac{5}{3}\varepsilon_n\right)\omega_{Di} - k^2\rho_s^2(\omega - \omega_{*i}(1+\eta_i))\left(\frac{\omega}{\omega_{*e}} + \frac{5}{3\tau}\varepsilon_n\right)\right] = f_t\frac{\omega_{*e}}{N_e}\left[\omega(1-\varepsilon_n) - \left(\frac{7}{3} - \eta_e - \frac{5}{3}\varepsilon_n\right)\omega_{De}\right] + 1 - f_t \tag{10}$$

where

$$\varepsilon_n = 2L_n/L_B, \quad \omega_{*ip} = \omega_{*i}(1+\eta_i)$$

$$N_j = \omega^2 - \frac{10}{3}\omega\omega_{Dj} + \frac{5}{3}\omega_{Dj}^2$$

Equation (10) shows explicitly the symmetry between ions and trapped electrons. This symmetry becomes complete in the limit $k^2\rho^2 = 0$ and $f_t = 1$. This is also the most unstable limit, since the free electrons have a stabilizing influence. The dispersion relation (10) has two branches that may be unstable. For $f_t = 0$ we recover the toroidal η_i branch, as described in Ref. [12]. The same branch, but with a reduced free electron response, is recovered for $N_e \gg N_i$, and the denominators N_e and N_i play a role which is similar to that of the denominators in the dispersion relation for a beam plasma system. Thus, for modes propagating in the ion drift direction, $N_i < N_e$, while for modes propagating in the electron drift direction, $N_e < N_i$. The modes become uncoupled when the inequalities are strong. Thus, for $N_i \gg N_e$ we obtain the new trapped electron branch described by the dispersion relation

$$\omega^2 + \omega\omega_{*e}\left[\frac{f_t}{1-f_t}(1-\varepsilon_n) - \frac{10}{3}\varepsilon_n\right] = -\frac{5}{3}\omega_{De}^2 - \frac{f_t}{1-f_t}\left(\eta_e - \frac{7}{3} + \frac{5}{3}\varepsilon_n\right)\omega_{*e}\omega_{De} \tag{11a}$$

This mode is symmetric to the η_i mode and becomes unstable at large η_e. It is similar to the toroidal collisionless η_e mode found by Horton et al. [7] (where the ion density perturbation is neglected), but it occurs when $k^2\rho^2 \ll 1$ and depends sensitively on the fraction of trapped electrons f_t. The new mode propagates in the ion drift direction for small ϵ_n and in the electron drift direction for larger ϵ_n (typical case), which behaviour is opposite to that of the η_i mode. It is also interesting to note that electron trapping introduces an instability that is driven by the electron temperature gradient (η_e). This is naturally associated with electron temperature relaxation, i.e. with electron heat diffusivity. Clearly, the pure trapped electron mode, just like the pure η_i mode, cannot produce particle transport. Thus, particle transport must be regarded as being due to coupling between the two branches. This is also true for the instability present at $\eta_i \sim \eta_e = \eta < 1$. For $f_t < 1$, the electron branch dominates at small η. If we denote the ion part of Eq. (10) by Δ, using $\xi = f_t/(1 - f_t - \Delta)$, and include it in Eq. (11a), we obtain the formal solution

$$\omega = -\frac{1}{2}\omega_{*e}\left[\xi(1-\varepsilon_n) - \frac{10}{3}\varepsilon_n\right] \pm \omega_{*e}\left[\frac{10}{9}\varepsilon_n^2 + \frac{1}{4}\xi^2(1-\varepsilon_n)^2 - \xi\varepsilon_n\left\{\eta_e + \frac{5}{3}\varepsilon_n(2-\varepsilon_n) - \frac{7}{3}\right\}\right]^{1/2} \tag{11b}$$

The ion response thus adds up to the adiabatic part of the electron response. For identifying an instability, it

is sufficient to substitute a real frequency into Δ. It then turns out that in the unstable regime for $\eta_i < 1$, $\eta_e < 1$, we have $\xi < 0$. This means that we have an instability which is driven by the compressibility effects that are otherwise stabilizing. In fact, the term $7\epsilon_n\xi/3$ arises from the sum of $\nabla\cdot\vec{v}$ and $\nabla\cdot\vec{q}$ effects in the energy equation. A particularly simple solution is obtained when ϵ_n approaches the upper stability limit for small η. In this case, $\omega \ll \omega_D$, so that for small $k^2\rho^2$

$$\Delta \approx \frac{\omega_{*e}}{N_i}\left(\frac{5}{3}\epsilon_n - \frac{7}{3}\right)\omega_{Di}$$

$$N_i \approx \frac{5}{3}\omega_{Di}^2$$

Then,

$$\xi \approx \frac{f_t}{1+\tau-f_t-\dfrac{7\tau}{5\epsilon_n}}$$

and Eq. (11b) turns into an explicit solution for a mode driven by compressibility effects when

$$f_t + \frac{7\tau}{5\epsilon_n} > 1+\tau$$

Furthermore, for $f_t < 1$ the η_i branch dominates at large ϵ_n. Then, neglecting the trapped electron response, we derive a stability criterion for large ϵ_n of the form

$$L_T > \frac{L_B}{(1-f_t)\dfrac{20}{9\tau} + \dfrac{\tau}{2(1-f_t)}} \qquad (12)$$

This stability criterion is of particular interest for explaining the good confinement in the H-mode regime where, typically, $\epsilon_n \gg 1$. The corresponding threshold for the pure η_i mode is obtained by taking $f_t = 0$ in Eq. (12). The latter condition is also obtained in the limit $\epsilon_n \gg 1$ from the more general threshold given in Ref. [12], as expressed explicitly in Ref. [11]. The stable regime for large ϵ_n is discussed in Ref. [3], where it is found to lead to stability near the axis. The implications for a threshold of this type for H-mode confinement are discussed in Refs [7-11], while the transition from dissipative type instabilities to reactive instabilities for large ϵ_n is discussed in Ref. [26]. For the derivation of a condition of the type given by Eq. (12) a theory valid for $L_n \gg L_B$ is required. In this limit, $\omega \sim \omega_D$, and thus no expansion in ω_D/ω is allowed. In this case it is necessary to use either a kinetic theory [7, 10] or the unexpanded fluid model presented in Refs [12] and [21], which is also discussed in Refs [3, 11, 24].

A recent comparison between these two models [24] shows that the thresholds are in good agreement for $\tau < 4$. For larger values of τ, the kinetic model gives a smaller η_i threshold, but a growth rate that is exponentially small in the region between the kinetic threshold and the fluid threshold. The kinetic instability in the intermediate regime is of a dissipative nature, so that condition (12) actually gives the condition for the onset of the strong reactive fluid instability. A stability plot for $f_t = 0.5$, $k^2\rho^2 = 0.1$ and $\eta_e = \eta_i = \eta$ is shown in Fig. 1.

The fluid approximations for the ion and the trapped electron responses used here are the same and so the level of accuracy of the present model should be the same as that given in Ref. [24] for the pure η_i mode. Nevertheless, it is appropriate to compare our model with the kinetic model.

One important effect of electron trapping is that it leads to an instability for $\eta_i \sim \eta_e = \eta \ll 1$. As pointed out above, this instability is mainly a trapped electron mode for which, however, coupling to the η_i branch is necessary. In Fig. 2b, where $\eta = 0.2$, it can be seen that in this region $\omega_r \ll \omega_{*e}$. Close to marginal stability,

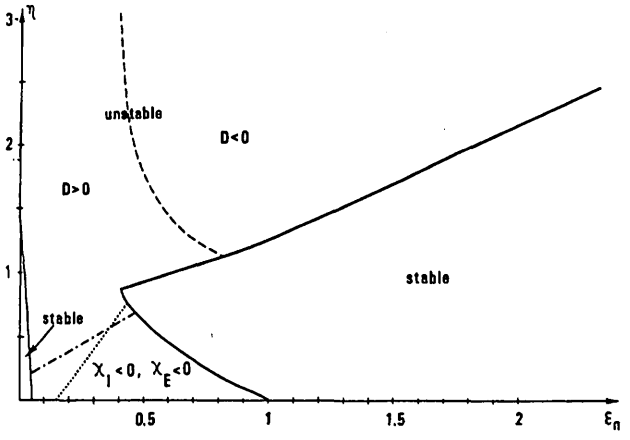

FIG. 1. Stability boundaries of η ($\eta = \eta_e = \eta_i$) as a function of ϵ_n ($= 2L_n/L_B$) for $\tau = 1$, $f_t = 0.5$ and $k^2\rho^2 = 0.1$. The signs of the diffusion coefficients are marked. In the region below the dotted line, $\chi_e < 0$; below the dash-dotted line, $\chi_i < 0$.

we also have $\gamma \ll \omega_{*e}$. Thus, with $\epsilon_n \sim 1$, we can use the expansion $|\omega| \ll |\omega_D|$. Reference [24] gives an analytical integration of the kinetic integral of the form

$$\frac{\delta n_j}{n} = \frac{q_j \phi}{T_j}\left[-1 + P\int_j + i\,\Delta\right] \tag{13a}$$

For $k^2\rho^2 \to 0$, the principal part is

$$P\int_j = 4\,\Gamma\left(\frac{\omega}{\omega_{Dj}} I_j^2 - \frac{\pi}{4} e^{-2\frac{\omega}{\omega_{Dj}}}\right) + 4\,\frac{\eta_j}{\epsilon_n}\,\frac{\omega}{\omega_{Dj}}\,I_j \tag{13b}$$

where

$$I_j = \int_0^1 e^{\frac{\omega}{\omega_{Dj}}(t^2-1)}\,dt$$

$$\Gamma_j = \frac{\omega}{\omega_{Dj}} - \frac{1}{\epsilon_n}\left[1 + \eta_j\left(2\,\frac{\omega}{\omega_{Dj}} - 1\right)\right]$$

and the resonant part is

$$\Delta_j = -4\sqrt{\frac{\pi\,\omega}{\omega_{Dj}}}\; e^{-\frac{\omega}{\omega_{Dj}}}\left(\Gamma_j I_j + \frac{\eta_j}{2\,\epsilon_n}\right) \tag{13c}$$

Here, we only consider marginal stability. Since $\omega > 0$ in this case, Δ_i is purely imaginary and contributes a real part to the response. For our present purposes, we may expand the expression for I:

$$I_j \approx 1 - \frac{2}{3}\,\frac{\omega}{\omega_{Dj}}$$

Omitting Δ_e we obtain the dispersion relation

$$\left(\frac{\omega}{\omega_{De}}\right)^2 - \frac{\frac{\pi}{4} + \frac{1}{\epsilon_n}\left(1 + \frac{\pi}{2}\right)}{n}\,\frac{\omega}{\omega_{De}} = \frac{\tau}{4}\,\frac{\xi - \frac{\pi}{\epsilon_n \tau}}{n} \tag{13d}$$

where

$$n = 1 + \frac{\pi}{2} + \frac{1}{\epsilon_n}\left(\frac{4}{3} + \frac{\pi}{2}\right)$$

$$\xi = \frac{1}{f_t}\left\{1 + \frac{1}{\tau} - P\int_i - i\,\Delta_i\right\}$$

Including now only terms up to $(\omega/\omega_*)^{3/2}$ in the ion response, we obtain $\omega_r/\omega_{*e} \sim 0.2$ for $\epsilon_n \sim 1$, $\tau = 1$, and the stability threshold is

$$-\frac{3.8}{\epsilon_n^2}\left(2 + \frac{1}{\epsilon_n}\right) + \frac{7.6}{\epsilon_n} + 10.9 > 0 \tag{13e}$$

or $\epsilon_{nth} \sim 0.8$.

Since we have omitted Δ_e, which gives a dissipative contribution, we have identified here a reactive instability with a threshold that is within 20% of the fluid threshold (see Fig. 1). Since Δ_e is destabilizing, the full kinetic threshold may be even closer to the fluid threshold.

Far from marginal stability ($\eta \gg 1$) and with $\epsilon_n \sim 1$, we have $|\omega| \gg |\omega_D|, |\omega_*|$. An expansion of Eq. (13a) up to order $\left(\frac{\omega_D}{\omega}\right)^2$, $\left(\frac{\omega_*}{\omega}\right)^2$ then gives (for $k^2\rho^2 = 0$)

$$\frac{\delta n_j}{n} = \left[-\frac{\omega_{*j}}{\omega} + \frac{\omega_{Dj}}{\omega}\left(1 - \frac{\omega_{*j}}{\omega}(1 + \eta_j)\right) + \frac{7}{4}\,\frac{\omega_{Dj}^2}{\omega^2}\right]\frac{q_j \phi}{T_j} \tag{13f}$$

Using quasi-neutrality, we obtain an analytical expression for the growth rate:

$$\gamma = \sqrt{\frac{1 + f_t}{1 - f_t}\left\{\epsilon_n(1 + \eta) - \frac{7}{4}\,\epsilon_n^2\right\} - \frac{(1 - \epsilon_n)^2}{4}} \tag{13g}$$

where $\tau = 1$ was used. For $\eta = 15$, $\epsilon_n = 2$ and $f_t = 0.5$, the ion mode dominates and we get $\gamma = 8.6$. The corresponding result from the fluid dispersion relation (Eq. (10)) is $\gamma = 7$, which is within 20% of the kinetic result.

A comparison can also be made with the kinetic results obtained by Romanelli and Briguglio [27]. The asymptotic slope (Fig. 3) obtained for $\tau = 1$ is $L_T = 0.5\,L_B$. With $f_t = (2\epsilon/(1 + \epsilon))^{1/2} = 0.577$, we obtain from Eq. (12) $L_T = 0.47\,L_B$.

Figures 2a and 2b show the eigenfrequencies for $\eta_e = \eta_i = 2$ and $\eta_e = \eta_i = 0.2$, respectively (from Eq. (10)). At the higher value the ion modes ($\omega_r/\omega_{*e} < 0$) dominate, while at the lower value the unstable modes

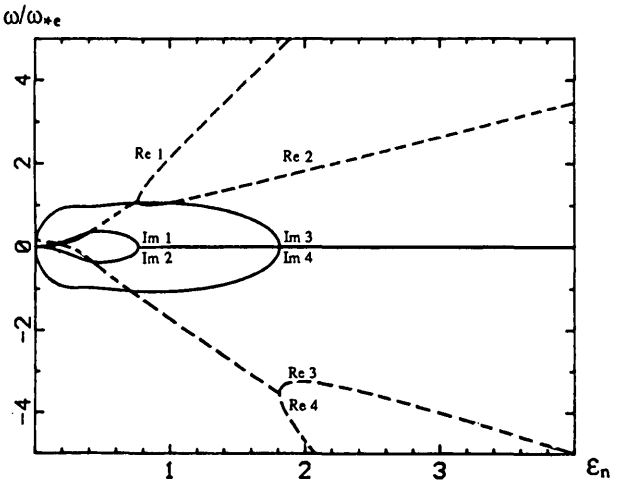

FIG. 2a. Eigenfrequencies (normalized to ω_{*e}) versus ϵ_n for $\eta = 2$, $\tau = 1$, $f_t = 0.5$ and $k^2\rho^2 = 0.1$.

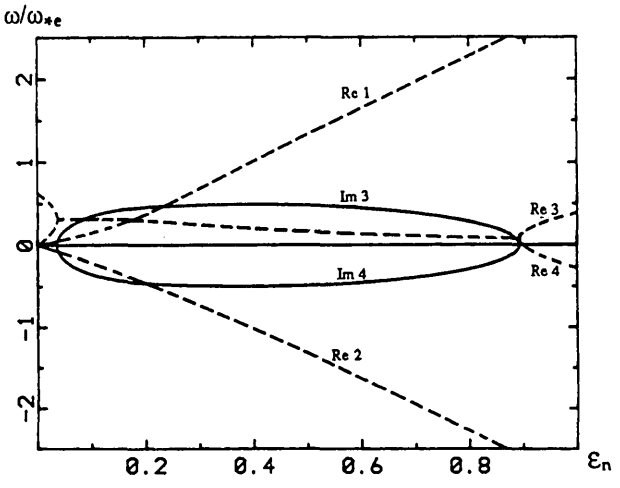

FIG. 2b. Eigenfrequencies (normalized to ω_{*e}) versus ϵ_n for $\eta = 0.2$, $\tau = 1$, $f_t = 0.5$ and $k^2\rho^2 = 0.1$.

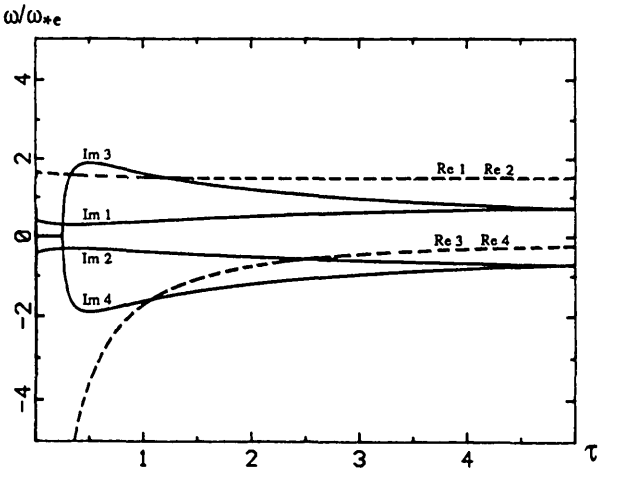

FIG. 2c. Eigenfrequencies (normalized to ω_{*e}) versus τ for $\eta = 3$, $\epsilon_n = 1$, $f_t = 0.5$ and $k^2\rho^2 = 0.1$.

have electron mode character ($\omega_r/\omega_{*e} > 0$). Figure 2c illustrates the τ-dependence of the mode frequencies (compare with Figs 8a, b).

4. QUASI-LINEAR DIFFUSION

For the quasi-linear diffusion, we proceed in the same way as in Ref. [11]. The thermal flux is obtained as

$$\vec{\Gamma}_{Tj} = \langle \delta T_j \vec{v}_E \rangle$$

where $\vec{v}_E$ is the $\vec{E} \times \vec{B}$ drift and δT_j is given by

$$\delta T_j = \frac{\omega}{\omega - \frac{5}{3}\omega_{Dj}} T_j \left[\frac{2}{3}\frac{\delta n_j}{n_j} - \frac{\omega_{*e}}{\omega}\left(\frac{2}{3} - \eta_i\right)\frac{e\phi}{T_e} \right] \tag{14}$$

The diffusion coefficient is then obtained by Fick's law:

$$\chi_j = -\Gamma_{Tj} / \frac{dT_j}{dr}$$

The saturation level is obtained by balancing the linear growth with the dominant convective non-linearity in the energy and continuity equations, i.e.

$$\gamma \delta T = \vec{v}_E \cdot \nabla \delta T \qquad \text{(energy equation)}$$

or

$$\gamma \delta n = \vec{v}_E \cdot \nabla \delta n \qquad \text{(continuity equation)}$$

Replacing now the gradient by a typical inverse length (in real space), we may cancel the temperature and density perturbations, thus obtaining the same condition from both equations. Expressing the inverse length as an effective k, we obtain the saturation level

$$\frac{e\phi}{T_e} = \frac{\gamma}{\omega_{*e}} \frac{1}{k_x L_n} \tag{15}$$

where x corresponds to the radial co-ordinate. Then, replacing the sums over k space by a single component, equal to the 'average' k, which we take to be the fastest growing mode, we obtain the following diffusion coefficients:

$$\chi_i = \frac{1}{\eta_i}\left[\eta_i - \frac{2}{3} - (1-f_t)\frac{10}{9\tau}\varepsilon_n - \frac{2}{3}f_t\Delta_i\right]$$

$$\times \frac{\gamma^3/k_x^2}{\left(\omega_r - \frac{5}{3}\omega_{Di}\right)^2+\gamma^2} \qquad (16a)$$

$$\chi_e = f_t\frac{1}{\eta_e}\left(\eta_e - \frac{2}{3} - \frac{2}{3}\Delta_e\right)\frac{\gamma^3/k_x^2}{\left(\omega_r - \frac{5}{3}\omega_{De}\right)^2+\gamma^2} \qquad (16b)$$

$$D = f_t\Delta_n\frac{\gamma^3/k_x^2}{\omega_{*e}^2} \qquad (16c)$$

where we can express Δ_j in terms of $\hat{\omega} = \omega/\omega_{*e}$:

$$\Delta_i = \frac{1}{N}\left\{|\hat{\omega}|^2\left[|\hat{\omega}|^2(\varepsilon_n - 1) + \hat{\omega}_r\varepsilon_n\left(\frac{14}{3} - 2\eta_e - \frac{10}{3}\varepsilon_n\right)\right.\right.$$
$$\left.+\frac{5}{3}\varepsilon_n^2\left(-\frac{11}{3} + 2\eta_e + \frac{7}{3}\varepsilon_n\right) - \frac{5}{3\tau}\varepsilon_n^2\left(1+\eta_e - \frac{5}{3}\varepsilon_n\right)\right]$$
$$\left.+\frac{50}{9\tau}\hat{\omega}_r\varepsilon_n^3(1-\varepsilon_n) - \frac{25}{9\tau}\varepsilon_n^4\left(\frac{7}{3} - \eta_e - \frac{5}{3}\varepsilon_n\right)\right\} \qquad (16d)$$

$$\Delta_e = \frac{1}{N}\left\{|\hat{\omega}|^2\left[|\hat{\omega}|^2(\varepsilon_n - 1) + \hat{\omega}_r\varepsilon_n\left(\frac{14}{3} - 2\eta_e - \frac{10}{3}\varepsilon_n\right)\right.\right.$$
$$\left.+\frac{5}{3}\varepsilon_n^2\left(-\frac{8}{3} + 3\eta_e + \frac{2}{3}\varepsilon_n\right)\right] + \frac{50}{9}\hat{\omega}_r\varepsilon_n^3(\varepsilon_n - 1)$$
$$\left.+\frac{25}{9}\varepsilon_n^4\left(\frac{7}{3} - \eta_e - \frac{5}{3}\varepsilon_n\right)\right\} \qquad (16e)$$

$$\Delta_n = \frac{1}{N}\left\{|\hat{\omega}|^2(1-\varepsilon_n) - \hat{\omega}_r\varepsilon_n\left(\frac{14}{3} - 2\eta_e - \frac{10}{3}\varepsilon_n\right)\right.$$
$$\left.-\frac{5}{3}\varepsilon_n^2\left(-\frac{11}{3} + 2\eta_e + \frac{7}{3}\varepsilon_n\right)\right\} \qquad (16f)$$

$$N = \left(\hat{\omega}_r^2 - \hat{\gamma}^2 - \frac{10}{3}\hat{\omega}_r\varepsilon_n + \frac{5}{3}\varepsilon_n^2\right)^2 + 4\hat{\gamma}^2\left(\hat{\omega}_r - \frac{5}{3}\varepsilon_n\right)^2 \qquad (16g)$$

These transport coefficients are in good agreement with fully non-linear mode coupling simulations, as will be shown later. In the limit $f_t \to 0$, we have $\chi_e = D = 0$, while χ_i becomes the thermal conductivity derived in Ref. [11]. The diffusion coefficients (16a–c) have the property discussed above, namely that L_n, L_{Ti} and L_{Te} tend to become equilibrated. If necessary, this can be accomplished by means of negative flows (pinch effects). The total pressure flux is, however, always outward, i.e.

$$\Gamma_p = \langle \delta p\, v_{EX}\rangle = n\,\Gamma_{Ti} + n\,\Gamma_{Te} + (T_i + T_e)\,\Gamma_n > 0 \qquad (17)$$

This condition, which is necessary for an overall relaxation, is always automatically fulfilled by the coefficients (16); in Section 5 it is shown to be rigorously fulfilled for the fully non-linear system. This also means that at most two of the fluxes Γ_{Ti}, Γ_{Te} and Γ_n can be negative. While particle pinch effects occur already for values of η that are only somewhat higher than one and are commonly observed in tokamaks, heat pinch effects typically require $\eta < 0.5$. They are likely to occur in pellet fuelling experiments where they may explain the observed rapid peaking of the temperature profile following the peaking of the density profile. A pure ion or electron heat pinch can occur if L_{Ti} and L_{Te} differ strongly. Again, of course, the pinch effect would have an equilibrating influence. The general coupling between particle transport and heat transport, roughly characterized by a tendency for equilibration of the scale lengths, gives the system a stiffness that may account for profile consistency.

For the energy flux, the stabilizing compressibility effects ($\nabla\cdot\vec{v}$ and $\nabla\cdot\vec{q}$) in the energy equation have a general tendency to lead to pinch effects. This is particularly pronounced for $\nabla\cdot\vec{v}$. For $\nabla\cdot\vec{q}$, this tendency is clear only for $f_t < 0.5$. An interesting aspect of the pinch effects is shown by

$$\Gamma_{Ti} = -\chi_i\frac{dT_i}{dr} =$$
$$-\left\{\frac{dT_i}{dr} - \left[\frac{2}{3} + (1-f_t)\frac{10}{9\tau}\varepsilon_n + \frac{2}{3}f_t\Delta_i\right]\frac{dn}{dr}\right\}$$
$$\times \frac{\gamma^3/k_x^2}{\left(\omega_r - \frac{5}{3}\omega_{Di}\right)^2+\gamma^2} \qquad (18a)$$

It can be seen that the heat pinch flux is proportional to the density gradient, while the outward flux is proportional to the temperature gradient. This means that we have a kind of competition between temperature relaxation and particle relaxation.

Similarly, for the particle flux we obtain

$$\Gamma_n = -f_t \frac{1}{N}\left\{\left[\,|\hat{\omega}|^2(1-\varepsilon_n) - \frac{2}{3}\varepsilon_n\omega_r(7-5\varepsilon_n) + \frac{5}{9}\varepsilon_n^2(11-7\varepsilon_n)\right]\frac{dn}{dr} - 2\varepsilon_n\left(\frac{5}{3}\varepsilon_n - \hat{\omega}_r\right)\frac{dT_e}{dr}\right\}\frac{\gamma^3/k_x^2}{\omega_{*e}^2} \qquad (18b)$$

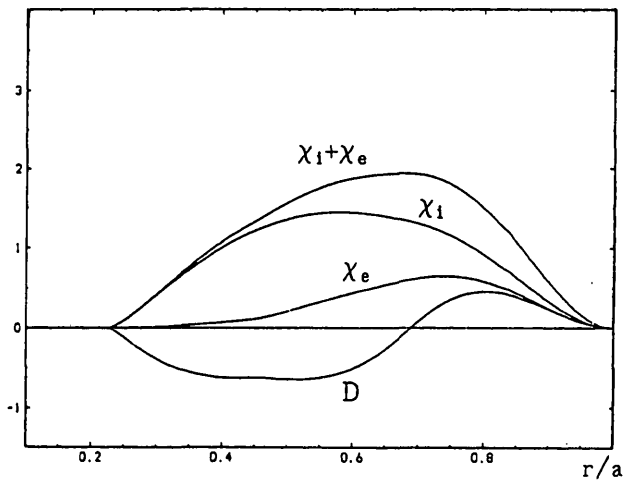

FIG. 3a. Radial variation of the quasi-linear diffusion coefficients for the TEXTOR profile [3] (τ = 1, $k^2\rho^2$ = 0.1, N = 1.91) with $f_t = (2\epsilon/(1+\epsilon))^{1/2}$, $\epsilon = r/R$.

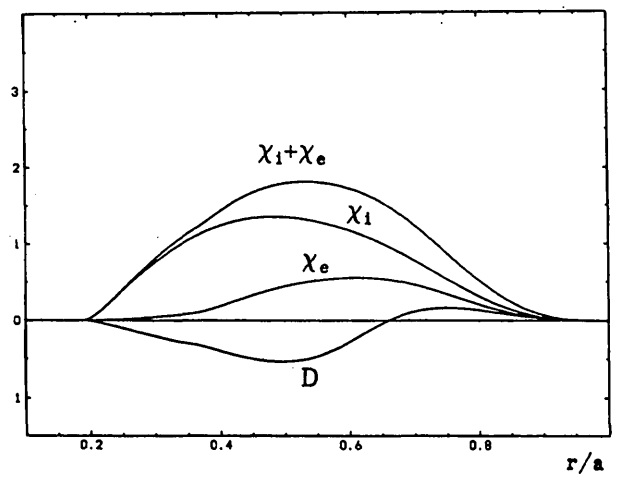

FIG. 3b. Radial variation of the quasi-linear diffusion coefficients for a JET profile (shot 8961) with off-axis RF heating and a central temperature of 2.64 keV.

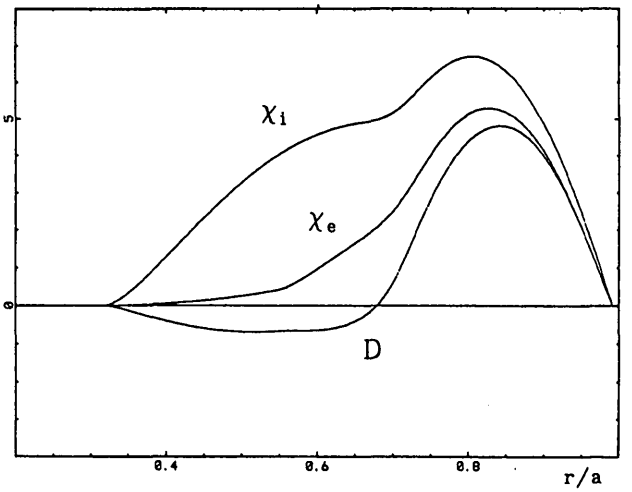

FIG. 3c. Radial variation of the quasi-linear diffusion coefficients for a JET profile (shot 16063) with combined neutral beam and RF heating. The central temperatures of the ions and electrons are 0.47 keV and 6.97 keV, respectively.

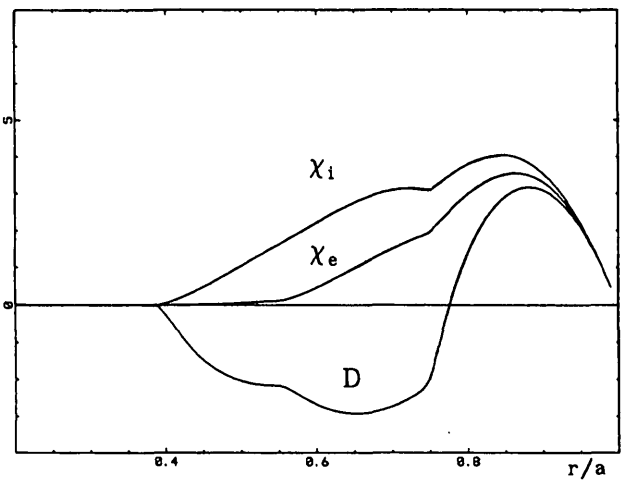

FIG. 3d. Radial variation of the quasi-linear diffusion coefficients for a JET profile (shot 17259) with only Ohmic heating and a very flat density profile. The central temperatures of the ions and electrons are 3.26 keV and 5.77 keV, respectively.

where the part proportional to dT_e/dr is inward when $\omega < 5\epsilon_n/3$, which is usually the case (it is always so for modes propagating in the ion drift direction).

This result is analogous to that obtained in Ref. [15] for the slab branch of η_i modes with dissipation. We note, however, that, in our case, also the flux proportional to dn/dr can become negative for large ϵ_n.

An interesting case regarding symmetry is that with large ϵ_n, $f_t \sim 1$, small $k^2\rho^2$, and with $\eta_i = \eta_e = \eta$ large enough for instability. In this limit the two branches have $\omega_{r1} \sim -\omega_{r2}$ and $\gamma_1 \sim \gamma_2$. In particular, for $\epsilon_n = 3$, $\eta = 3.9$, $k^2\rho^2 = 0.0001$ and $f_t = 1$ we find the solution $\omega_{r1} = -\omega_{r2} = 40$ and $\gamma_1 = \gamma_2 = 10$. In this case,

both branches give particle pinch effects, although the part proportional to dT_e/dr for the electron branch leads to outward diffusion ($D/\chi_e = -3$).

We have evaluated the radial profiles of the diffusion coefficients (16) for a few experimental n and T profiles. Figure 3a shows a TEXTOR profile with only Ohmic heating (from Ref. [3]) and Fig. 3b shows a JET profile with off-axis RF heating.

In the TEXTOR case, also the dissipative trapped electron mode is active (collision dominated) and so χ_e and D have to be modified. However, when the particle diffusion coefficient D derived here (Eq. (16c)) is added to that obtained from the dissipative trapped electron mode, rough agreement with the experimentally observed particle transport is obtained. For the JET profile in Fig. 3b we also expect collisions to be important and we note that the diffusivity profiles are very similar to the TEXTOR profiles. We have verified that the magnitudes of χ_i and χ_e are correct in the most interior part. The JET profiles in Figs 3c and 3d are qualitatively different and correspond to higher temperatures. The better trend for the radial variation of χ_i and χ_e indicates that, in this case, JET is in the collisionless regime where the present model applies. The JET discharge in Fig. 3d has a very flat density profile and also a rather flat temperature profile. Although this is an Ohmic shot, it has the appearance of an H-mode shot and the energy transport is comparatively small.

The overall very good agreement between the results obtained with our model and the general experimental trends can probably be explained partly by the fact that in the fluid model no further approximations such as numerical fitting are necessary. Another reason could be that the kinetic resonance part of the growth rate (neglected in Eq. (16)) is saturated on a shorter timescale because of diffusion in velocity space.

5. SIMULATION RESULTS

The results discussed in this section are based on a numerical simulation of system (9). The emphasis is on the scaling properties of the diffusion coefficients and their relation to the quasi-linear results of Section 4. Transforming into dimensionless variables in k-space, the model equations can be written

$$\frac{d}{dt}\,\delta n_{etk} = -\,i\,k_y\,f_t\,\phi_k - i\,k_y\,\varepsilon_n \times \{\,\delta n_{etk} + f_t\,\delta T_{etk} - f_t\,\phi_k\,\} - \gamma_d\,\delta n_{etk} \tag{19a}$$

$$\frac{d}{dt}\,\delta T_{etk} = -\,i\,k_y\,\eta_e\,\phi_k - i\,k_y\,\varepsilon_n \times \left\{ -\frac{2}{3}\,\phi_k + \frac{7}{3}\,\delta T_{etk} + \frac{2}{3\,f_t}\,\delta n_{etk} \right\} - \gamma_d\,\delta T_{etk} \tag{19b}$$

$$\frac{\partial}{\partial t}\,(1 - f_t + k^2)\,\phi_k = -i\,k_y \left(1 - f_t - \frac{1+\eta_i}{\tau}\,k^2\right)\phi_k + i\,k_y\,\varepsilon_n \{\,(1-f_t)\,(1 + 1/\tau)\,\phi_k + \delta T_{ik} + (1 + 1/\tau)\,\delta n_{etk} + f_t\,\delta T_{etk}\} + \sum_{k_1} (\vec{k}_1 \times \vec{k}_2)\cdot\vec{e}_{\|}\,\frac{k_2^2 - k_1^2}{2}\,\phi_{k_1}\,\phi_{k_2} \tag{19c}$$

$$\frac{d}{dt}\,\delta T_{ik} = -\,i\,k_y\,\frac{1}{\tau}\left[\eta_i - \frac{2}{3\tau}\,(1+\eta_i+\tau)\,k^2\right]\phi_k + i\,k_y\,\frac{\varepsilon_n}{\tau}\left\{\frac{2}{3\tau}\,(1 - f_t + \tau)\,\phi_k + \frac{7}{3}\,\delta T_{ik} + \frac{2}{3\tau}\,\delta n_{etk}\right\} - i\,k_y\,\frac{2}{3\,\tau^2}\,\varepsilon_n\,k^2 \times \left\{(1+\tau)\,\phi_k + \frac{\tau}{1-f_t}\,\delta T_{ik} + \frac{1+\tau}{1-f_t}\,\delta n_{etk} + \frac{f_t\,\tau}{1-f_t}\,\delta T_{etk}\right\} \tag{19d}$$

where

$$\frac{df}{dt} = \frac{\partial f}{\partial t} - \sum_{k_1} (\vec{k}_1 \times \vec{k}_2)\cdot\vec{e}_{\|}\,\phi_{k_1}\,f_{k_2}$$

and the fields have been normalized as

$$\phi = \frac{e\bar{\phi}/T_e}{\rho_s/L_n}\,,\quad \delta T_j = \frac{\delta\bar{T}_j/T_e}{\rho_s/L_n}\,,\quad \delta n_{et} = \frac{\delta n_{et}/n_o}{\rho_s/L_n}$$

The unit of time is $\omega^{-1} = L_n/c_s$ and the unit of length is ρ_s.

System (19) obeys the turbulent conservation laws

$$\frac{1}{2}\frac{\partial}{\partial t}\sum_k\left\{|\delta n_{et}|^2+\frac{3f_t^2}{2}|\delta T_{et}|^2\right\}$$
$$=f_t(1-\varepsilon_n)\tilde{D}+\frac{3f_t}{2}\left(\eta_e-\frac{2\varepsilon_n}{3}\right)\eta_e\tilde{\chi}_e$$
$$-\sum_k\gamma_d\left\{|\delta n_{et}|^2+\frac{3f_t^2}{2}|\delta T_{et}|^2\right\} \quad (20)$$

$$\frac{1}{2}\frac{\partial}{\partial t}\sum_k\{(1-f_t)+k^2\}|\phi|^2$$
$$=\frac{n_i\varepsilon_n}{\tau}\tilde{\chi}_i+\varepsilon_n\left(1+\frac{1}{\tau}\right)\tilde{D}+n_e\varepsilon_n\tilde{\chi}_e$$
$$-\sum_k\gamma_d\{(1-f_t)+k^2\}|\phi|^2 \quad (21)$$

where use has been made of the conservation property of convective non-linearities, i.e.

$$\int d^3x\, f(\vec{e}\times\nabla\varphi)\cdot\nabla f=0$$

for any f. Here, the instantaneous diffusivities (not averaged) enter. Relation (21), applied to a stationary state (i.e. $\partial/\partial t = 0$), shows that the total flux, $\Gamma_P = \langle\delta P\, v_{Ex}\rangle$, is always positive (outward).

The numerical simulations are performed in the same way as those reported in Ref. [11]. Starting with a k-spectrum with randomly distributed phases at noise level, the time integration of Eq. (19) has been performed with a predictor-corrector method. A fully de-aliased spectral method has been used, with a 64×64 grid, spanning $-1.8 \le k_x, k_y \le 1.8$. The time step has been chosen to maintain the conservation relations (20, 21) to within a few per cent. We have taken the background profiles to be stationary, i.e. quasi-linear saturation mechanisms are omitted.

The incorporation of artificial damping rates is discussed in Refs [11, 22], and only a brief account is given here. We have used an absorbing mantle at high wave numbers to truncate the spectrum, i.e. $\gamma = \gamma_\infty$ above $k = k_\infty$. Here, $k_\infty = 1.5$ and $\gamma_\infty = 2$ are found to be convenient. The inclusion of the non-linear ion polarization drift is known to lead to inverse cascading, thus making low-k damping necessary for a stationary state to develop. As in earlier treatments [11, 22], we have used $\gamma = \gamma_0(1 - k_\perp^2/k_0^2)$ for $|k_\perp| < k_0$, where $k_0 = 0.5$ and $\gamma_0 = 0.6$ in our simulations. We focus here on the scaling properties of the diffusion coefficients and the validity of quasi-linear theory. Dimensional considerations show that the diffusivities must scale as

$$D,\ \chi_{e,i} = \frac{\rho_s^2 c_s}{L_n} f(\eta_{i,e}, \varepsilon_n, \tau, f_t) \quad (22)$$

The scalings with temperature (for a given value of τ) and magnetic field are thus fixed as

$$D,\ \chi_{e,i} \approx T_e^{3/2}/B^2 \quad (23)$$

Here, the scaling properties of the function f are investigated. We consider L_B as a constant and write $L_n = \epsilon_n L_B/2$ in Eq. (22).

In Fig. 4a, the time evolution of the normalized perturbation fields is followed for $\eta_i = 3$, $\tau = \epsilon_n = 1$ and $f_t = 0.5$. Figure 4b shows the k_y spectrum (integrated over k_x) of the potential. The turbulence is fairly isotropic as a result of non-linear isotropizing. The corresponding values of the diffusivities (in units of $\rho_s^2 c_s/L_n$) are given by $\chi_e = 1.8$, $\chi_i = 15.3$ and $D = -3.2$. The ion thermal conductivity is the dominant loss mechanism, as is usually the case for positive heat fluxes.

Figure 5a confirms the presence of heat pinch effects for small $\eta = \eta_i = \eta_e$. The quasi-linear expressions give good agreement with the simulations down to values of $\epsilon_n \sim 0.4$, as shown in Fig. 5b. For the present value of η, only the trapped electron branch is unstable. The growth rate becomes comparable to the real frequency for $\epsilon_n \sim 0.2$, thus making quasi-linear results questionable for small ϵ_n. The corresponding scalings for $\eta = 2$ are given in Fig. 6a and the quasi-linear results in Fig. 6b. Here, the η_i mode dominates, except for $\epsilon_n < 0.2$. Both the quasi-linear results and the simulations show the presence of a particle pinch. The chosen parameter values correspond to typical tokamak profiles, so that the observed particle pinch is relevant for present-day tokamaks (see Figs 3a–3d).

The favourable ϵ_n scaling of χ_i in the case of pure η_i modes [11] is also found for the other diffusion coefficients. The increase of ϵ_n towards the central tokamak region enhances the possibility of achieving radial profiles of D and χ in agreement with experiments.

Furthermore, the fraction of trapped electrons f_t is also a function of radius and varies as $f_t = (2\epsilon/(1+\epsilon))^{1/2}$, $\epsilon = r/R$. This will destabilize the modes towards the edge and also increase the transport in this region. This is shown in Fig. 7a for $\eta = 2$ and $\tau = \epsilon_n = 1$; the quasi-linear results are given in Fig. 7b. Linear theory suggests that the quasi-linear expressions are valid for $f_t < 0.7$, which is in good agreement with the obtained results. However, the inclusion of electron trapping has made the instability stronger, thus limiting the region of applicability of quasi-linear theory.

The scaling of the diffusivities with τ is presented in Figs 8a and 8b. The results show a favourable scaling

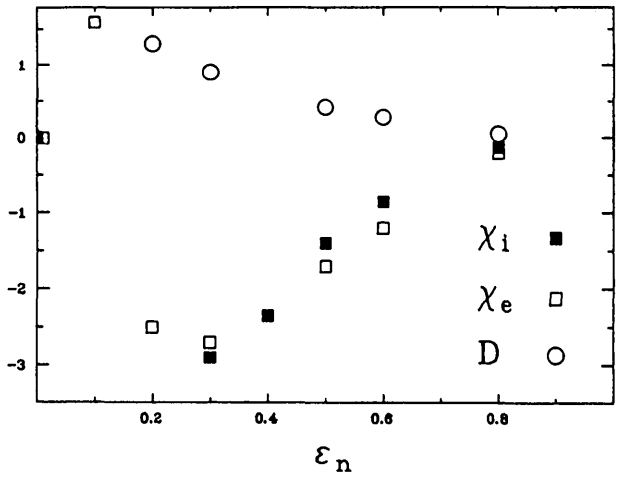

FIG. 5a. Numerically obtained ϵ_n scaling of the diffusion coefficients for $\eta = 0.1$, $\tau = 1$ and $f_t = 0.5$.

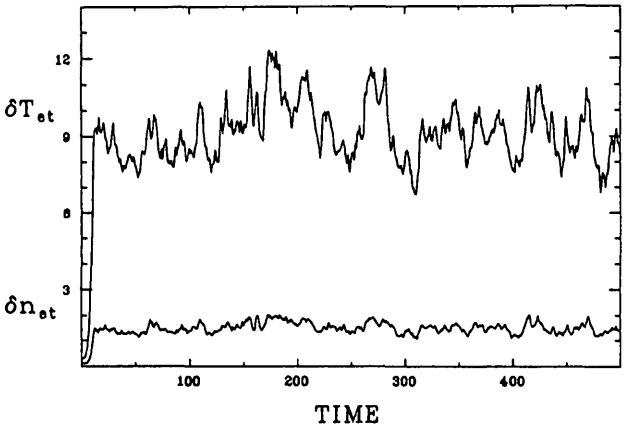

FIG. 4a. Time evolution of the trapped electron density and temperature perturbations for $\eta_i = 3$, $f_t = 0.5$ and $\tau = \epsilon_n = 1$.

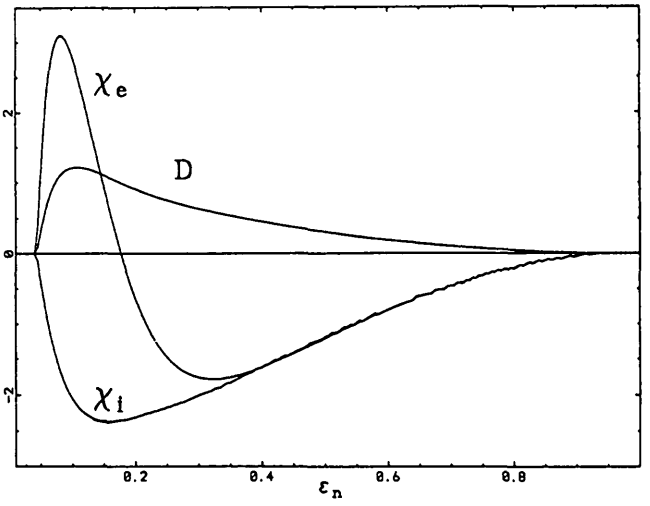

FIG. 5b. Quasi-linear results for the parameter values given in Fig. 5a.

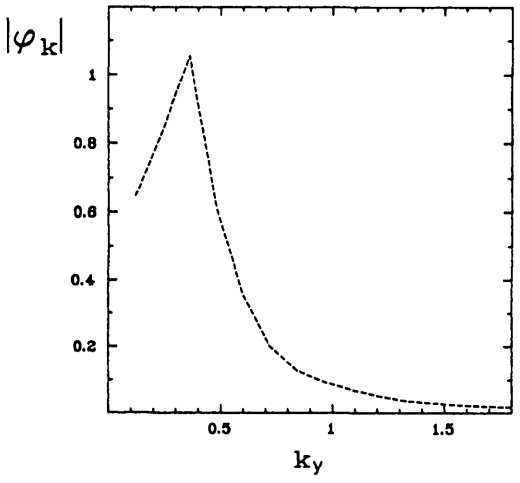

FIG. 4b. Spectrum of the potential perturbations (k_x integrated) corresponding to Fig. 4a.

of the energy transport with τ, favouring tokamak operation in the hot ion mode. This effect is more pronounced for the pure η_i mode [11], since in this case the contribution of the trapped electron mode to the transport is relatively large for $\tau < 1$.

6. DISCUSSION

As pointed out in the Introduction, the reactive type of drift modes considered in this work is of a very fundamental nature for magnetic confinement systems.

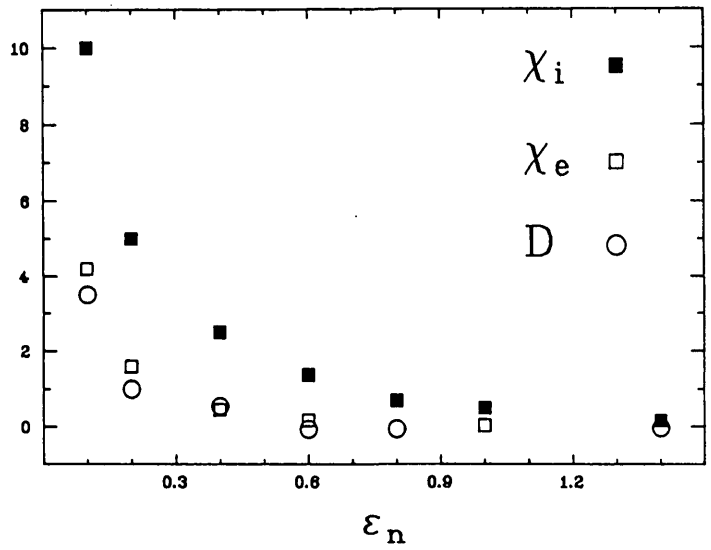

FIG. 6a. Variation of the diffusivities with ϵ_n for $\eta = 2$, $\tau = 1$ and $f_t = 0.5$ as obtained by numerical simulations.

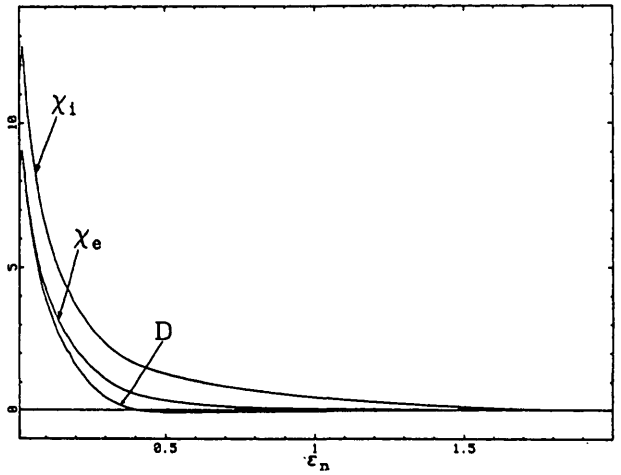

FIG. 6b. Quasi-linear results for the parameter values given in Fig. 6a.

The fully toroidal fluid model used here has made it possible to simulate the fully non-linear turbulence of these modes, driven by temperature gradients and compressibility, without expanding in L_n/L_B or in ω_D/ω, also when electron trapping is included. The inclusion of electron trapping has revealed a collisionless trapped electron mode that is symmetric to the η_i mode and that is driven by the electron temperature gradient. In the limit of vanishing FLR and when all electrons are trapped, the linear system becomes completely symmetric regarding the electron and ion species. At the same time, however, another type of symmetry appears. This is a tendency for large heat flows when $\eta_i = \eta_e = \eta > 1$ and for large particle flows when $\eta < 1$. This tendency also remains for realistic numbers of trapped electrons. When the deviation from $\eta = 1$ becomes large, negative particle fluxes may arise for $\eta > 1$ and negative heat fluxes may arise for $\eta < 1$. For typical values of the fraction of trapped electrons f_t, particle pinch effects occur already at moderate values of η and ϵ_n, as exist in most tokamak discharges, while the heat pinch occurs typically at $\eta < 0.5$. Heat pinch effects are thus expected to occur only in rather extreme conditions, for example when pellet fuelling

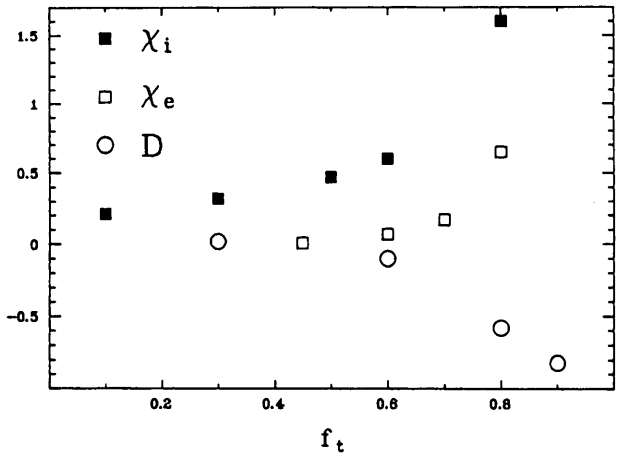

FIG. 7a. Numerically obtained scalings of χ_i, χ_e and D with the fraction of trapped electrons f_t, for $\eta = 2$, $\tau = 1$ and $\epsilon_n = 1$.

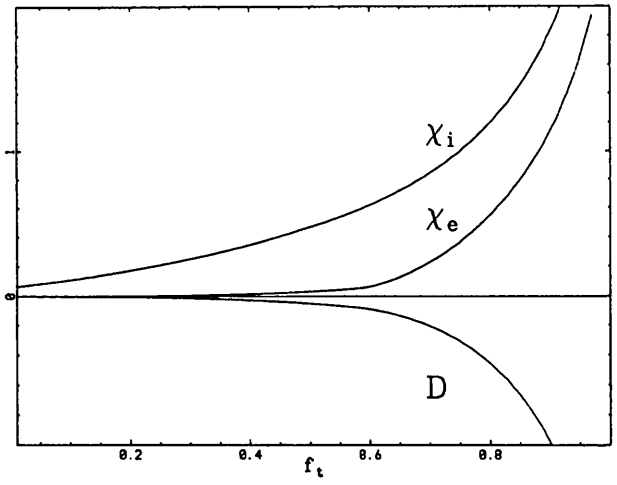

FIG. 7b. Quasi-linear results for the parameter values given in Fig. 7a.

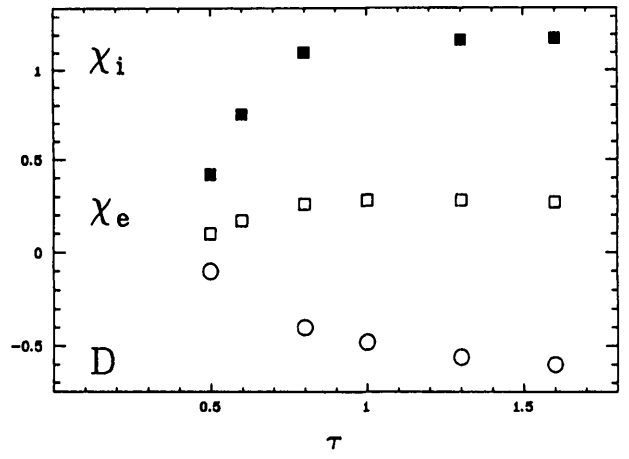

FIG. 8a. Numerically obtained scalings of χ_i, χ_e and D with τ for $\eta = 3$, $\epsilon_n = 1$ and $f_t = 0.5$.

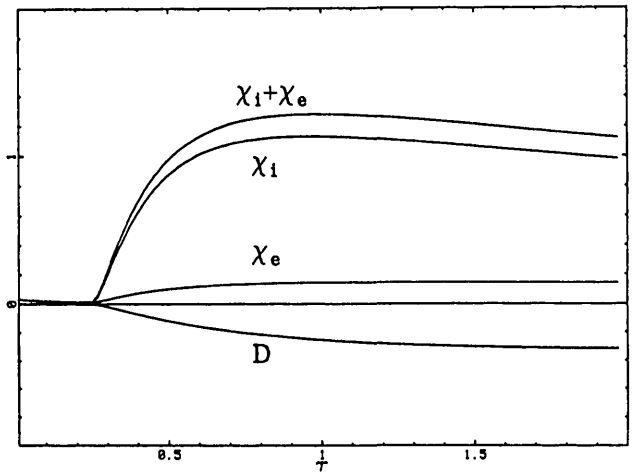

FIG. 8b. Quasi-linear results for the parameter values given in Fig. 8a.

is applied. This conception is also supported by the experimentally observed rapid peaking of the temperature profile following the peaking of the density profiles. Another effect of trapping is that the favourable dependence of the transport on T_i/T_e is reduced. For realistic values of f_t, we typically have $\chi_i > \chi_e$ also for $T_i = T_e$. This tendency has recently been observed experimentally [28, 29]. In fact, the relation $\chi_i \sim 2\chi_e$ seems to be rather typical in the bulk of the plasma (see Figs 3a and 3b), as reported in Refs. [28, 29]. Moreover, the trend of $\chi_i > 2\chi_e$ in the inner region is also evident from Fig. 1a of Ref. [29]. A number of general features of η_i mode transport, in particular a favourable dependence on T_i/T_e, have also been observed [30]. To improve the radial dependence in the outer region, electron–ion collisions should also be included. The general tendency for equilibration of L_n and L_T is also interesting as regards thermodynamics. Also of interest is a comparison of the present mode with the MHD ballooning mode, which is similar to the toroidal η_i mode in several respects and which limits the pressure gradient, leaving free the relative contributions from density and temperature gradients. The present system which contains two reactive drift modes removes this degeneracy and the results also correlate well with recent main experimental trends regarding transport in tokamaks.

REFERENCES

[1] ROMANELLI, F., TANG, W.M., WHITE, R.B., Nucl. Fusion **26** (1986) 1515.
[2] DOMINGUEZ, R.R., WALTZ, R.E., Nucl. Fusion **27** (1987) 65.
[3] ROGISTER, A., HASSELBERG, G., WAELBROECK, F., WEILAND, J., Nucl. Fusion **28** (1988) 1053.
[4] EJIMA, S., and Doublet III Group, Nucl. Fusion **22** (1982) 1627.
[5] GREENWALD, M., GWINN, D., MILORA, S., et al., Phys. Rev. Lett. **53** (1984) 352.
[6] SÖLDNER, F.X., MÜLLER, E.R., WAGNER, F., et al., Phys. Rev. Lett. **61** (1988) 1105.
[7] HORTON, W., HONG, B.G., TANG, W.M., Phys. Fluids **31** (1988) 2971.
[8] DOMINGUEZ, R.R., WALTZ, R.E., Phys. Fluids **31** (1988) 3147.
[9] ROMANELLI, F., Phys. Fluids, B **1** (1989) 1018.
[10] BIGLARI, H., DIAMOND, P.H., ROSENBLUTH, M.N., Phys. Fluids, B **1** (1989) 109.
[11] NORDMAN, H., WEILAND, J., Nucl. Fusion **29** (1989) 251.
[12] JARMÉN, A., ANDERSSON, P., WEILAND, J., Nucl. Fusion **27** (1987) 941.
[13] MANHEIMER, W.M., ANTONSEN, T.M., Phys. Fluids **22** (1979) 957.
[14] COPPI, B., Comments Plasma Phys. Controll. Fusion **5** (1980) 261.
[15] ANTONSEN, T., COPPI, B., ENGLADE, R., Nucl. Fusion **19** (1979) 641.
[16] TERRY, P.W., Phys. Fluids, B **1** (1989) 1932.
[17] KADOMTSEV, B., POGUTSE, O., Sov. Phys. — JETP **24** (1967) 1172.
[18] COPPI, B., REWOLDT, G., Phys. Rev. Lett. **33** (1974) 1329.
[19] COPPI, B., PEGORARO, F., Nucl. Fusion **17** (1977) 969.
[20] LIU, C.S., Phys. Fluids **12** (1969) 1489.
[21] ANDERSSON, P., WEILAND, J., Phys. Fluids **31** (1988) 359.
[22] WALTZ, R.E., Phys. Fluids **29** (1986) 3684.
[23] COPPI, B., Phys. Lett., A **128** (1988) 193.
[24] NILSSON, J., LILJESTRÖM, M., WEILAND, J., in Controlled Fusion and Plasma Physics (Proc. 16th Eur. Conf. Venice, 1988), Vol. 13B, Part IV, European Physical Society (1988) 1417.

[25] ANDERSSON, P., A Fully Toroidal Fluid Analysis of Electrostatic Ballooning Modes including Trapped Electrons, Preprint CTH-IEFT/PP-1986-17, Chalmers University of Technology, Göteborg (1986).
[26] TANG, W.M., REWOLDT, G., CHEN, L., Phys. Fluids **29** (1986) 3715.
[27] ROMANELLI, F., BRIGUGLIO, S., in Controlled Fusion and Plasma Physics (Proc. 16th Eur. Conf. Venice, 1988), Vol. 13B, Part I, European Physical Society (1988) 355.
[28] McGUIRE, K.M., ARUNASALAM, V., BARNES, C.W., et al., Plasma Phys. Controll. Fusion **30** (1988) 1391.
[29] FONCK, R.J., HOWELL, R., JAEHNIG, K., et al., Ion Thermal Confinement in the TFTR Enhanced Confinement Regime, Preprint PPPL-2573, Princeton Plasma Physics Laboratory, Princeton, NJ (1988).
[30] ZARNSTORFF, M.C., GOLDSTON, R.J., BELL, M.G., et al., in Controlled Fusion and Plasma Physics (Proc. 16th Eur. Conf. Venice, 1988), Vol. 13B, Part I, European Physical Society (1988) 35.

(Manuscript received 6 July 1989
Final manuscript received 1 February 1990)